CHINESE OPTICS LETTERS

Vol. 21, No. 3 | March 2023

Self-healing of holographically generated moiré lattice wave fields

Siwei Tang (唐思维)[1], Chunlei Shang (尚春雷)[1], Zhaofeng Liu (刘兆峰)[1], Chengzhen Lu (卢城臻)[1], Yangjian Cai (蔡阳健)[1,2*], Yuanmei Gao (高垣梅)[1**], and Zengrun Wen (温增润)[1***]

[1] Shandong Provincial Engineering and Technical Center of Light Manipulations & Shandong Provincial Key Laboratory of Optics and Photonic Device, School of Physics and Electronics, Shandong Normal University, Jinan 250358, China

[2] School of Physical Science and Technology, Soochow University, Suzhou 215006, China

*Corresponding author: yangjiancai@sdnu.edu.cn

**Corresponding author: gaoyuanmei@sdnu.edu.cn

***Corresponding author: wenzengrun@163.com

Received July 31, 2022 | Accepted September 20, 2022 | Posted Online October 12, 2022

Self-healing in optics generally refers to the ability to reconstruct itself and restore the original state after encountering obstacles in the propagation of the light field. In this research, we observe the processes of the wave fields from perfect to defect in front of the focal plane of the 4f system, finally returning to an intact situation after the plane. According to simulations and experimental results, there is a minimum self-healing distance for the moiré lattice field that positively associates with the radius of the defect (obstacle) in the nondiffracting transmission range. Furthermore, it is observed that the defect self-healing is a process of "repairing the center and then repairing the edges." These findings can be applied in areas such as optical imaging, capture, and information processing.

Keywords: moiré lattice; nondiffraction; self-healing wave field.
DOI: 10.3788/COL202321.030502

1. Introduction

In recent years, the remarkable properties of a beam for self-healing in the nondiffraction range have attracted widespread attention[1–4]. Self-healing in optics refers to the characteristics of a beam that can self-reconstruct and return to its initial state after encountering opaque obstacles, which was first discovered in the Bessel beam[5], although the concept was not yet formally proposed at the time. The Bessel beam is an exact solution of the Helmholtz equation under the 0th-order Bessel function, and its lateral light intensity distribution does not change with propagation, so it is called a nondiffracted beam[6]. The ideal nondiffractive beam has infinite energy and cannot be realized in actuality. Experimentally, the Bessel beam obtained is an approximately nondiffractive beam due to the limitation of the aperture, and its nondiffractive propagation distance $Z_{\max}$ depends on the size of the aperture[7]. By utilizing geometric optics, the self-healing was explained by the fact that the obstacle forms a conical shadow in the direction of propagation, the scope of which depends solely on the radius of the obstacle. The light fields will reconstruct the original structure once the transmission distance exceeds the obstacle shadow[2,8,9].

Beyond the Bessel beams, the self-healing has been expanded in the nondiffracting beams[1]. Vaity *et al.*[10] experimentally confirmed the self-healing properties of a single-ring lattice beam. The self-reconstruction in this study can be understood by observing the Poynting vector or the transverse energy flow in different z planes. Later, the self-healing properties of pillar array optical fields and high-power discrete vortex beams were investigated[11,12]. Further, some basic nondiffracting beams also possess self-healing properties, such as Mathieu beams[13], transverse parabolic beams[14–16], and beams generated by plane wave interference of conical wave vectors[17–19]. They all have a common feature, namely, the spectral components are located on a circle with a cone-shaped wave vector, and the light field is essentially superimposed by the cone waves. This rule is satisfying, since it anticipates the self-healing characteristics of nondiffracting lattice wave fields.

Moiré lattice wave fields are periodic or aperiodic patterns produced by superimposing periodic fundamental lattice wave fields with a certain twisted angle[20]. As a kind of discrete nondiffracting beam, moiré wave fields induced photonic lattices to exhibit several interesting physical properties, such as defects (vacancies) and dark singularities[21,22], localization delocalization transition[23,24], and spatial solitons[25]. In previous work, holographic methods for generating moiré wave fields have been proposed and the nondiffraction properties of the wave fields have been measured simultaneously[26,27]. The self-healing

property in the holographically generated moiré wave field is still a topic to be studied.

In this work, the self-healing properties of holographically generated moiré lattice wave fields are studied through simulations and experiments. By altering the size, shape, and location of the defect, the self-healing phenomena are given out, showing that the minimum self-healing distance of the moiré lattice wave fields is positively correlated with the radius of the obstacle (or defect), which conforms to the self-healing law of the Bessel-like beam[1,28]. In addition, the moiré lattice wave-field propagation before the back focal plane of the 4f system is also measured.

2. Self-Healing Mechanism and Experimental Methods

2.1. Self-healing mechanism of nondiffracted beam

The conical wave-field dynamics demonstrates the self-healing mechanism of the nondiffracting beam[8,9], as shown in Fig. 1. The wave vector of the circular light source is k, and has an angle θ with the z axis. An opaque obstacle with a radius of R is placed on the propagation path, forming a conical shelter area (obstacle shadow) length, $Z_{\min}$ behind the obstacle. The light field behind the lens is the superposition field of the conical wave. In the maximum nondiffracted transmission distance $Z_{\max}$, the unblocked light waves will reconstruct the original structure behind the sheltered area[2,8].

Assume that the obstacle is located at $z=0$, the complex amplitude of the incident light field is U_0, the complex amplitude of the light field disturbed by the obstacle is U_D, and the complex amplitude of the light field diffused at the complementary screen (aperture) is U_C. According to the Babinet principle, $U_D = U_0 - U_C$. U_C is inversely proportional to z, according to the literature[7]. When transmitted to infinity, U_C becomes 0, The intensity of the light field disturbed by an obstacle in the far-field diffraction region is expressed as $\lim_{z\to\infty}|U_D|^2 = |U_0|$.

Therefore, the initial intensity distribution will be reconstructed in the far field when the ideal nondiffractive beam is disturbed by an obstacle. The self-healing range is ($Z_{\min}$, $Z_{\max}$), and the lowest self-healing distance is $Z_{\min}$ if the incident beam is an ideal nondiffraction beam. According to geometric relations, we obtain

$$Z_{\min} = \frac{R}{\tan\theta}. \tag{1}$$

It can be seen that for a given beam, θ is determined, and the minimum self-healing distance only depends on the radius R of the obstacle.

From the viewpoint of wave optics, Aiello *et al.*[28] rederived the above mechanism independent of geometric parameters and obtained the exact solution for the minimum self-healing distance of the conical wave field,

$$Z'_{\min} = \sqrt{2}\frac{R}{\tan\theta} = \sqrt{2}Z_{\min}. \tag{2}$$

The results obtained by the above two methods are highly consistent. Moreover, this result can be extended to scalar and vector Bessel–Gaussian beams[28,29]. According to the above results, some basic self-healing properties of the nondiffracted lattice wave field are predicted. First, the light field will reconstruct its original structure within the nondiffracting distance, as long as the obstacle is not too large. Second, the larger the obstacle, the longer the minimum self-healing distance.

2.2. Experimental setup

The moiré lattice wave field is generated by using the holographic method (also known as the one-step imaging method), a common method for complex interference beams. The experimental device is shown in Fig. 2. The light modulated by the pure-phase spatial light modulator (SLM) passes through a 4f system consisting of polarizer P2 and lenses L3, L4 to generate the desired moiré lattice wave field. A ring filter matches the spectral distribution and is positioned on the spectral plane of the 4f system. Finally, the intensity distribution of the wave field is recorded by a CCD camera near the rear focal plane of the 4f system. Two orthogonal polarizers, P1 and P2, are used to eliminate background light and enhance the contrast of the wave field. An obstacle is placed in the path of the beam but is not required when examining the self-healing of the wave fields with defects. We just load the phase diagram with a defect on the SLM

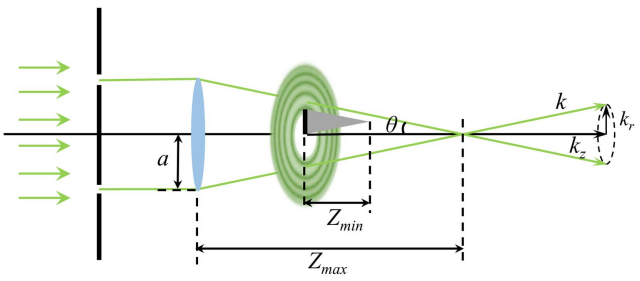

Fig. 1. Self-healing mechanism of the conical wave-fields.

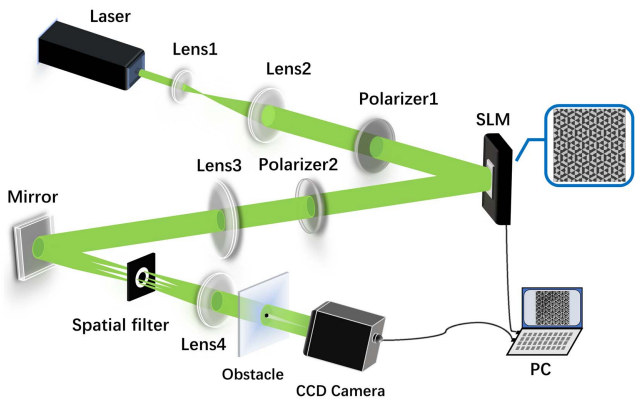

Fig. 2. Schematic of experimental setup on self-healing moiré wave fields. CCD, charge-coupled device; SLM, spatial light modulator.

and move the CCD around f_0 (the focal plane of L4) along the z axis to record the wave field at different positions.

2.3. Theoretical analysis and simulation

In Fig. 2, in the front focal plane of the Fourier transform lens, there are two groups of six-point light sources that make up a regular hexagon; one of the hexagons introduces the π phase difference. Twelve-point light sources are on a circle with a radius of a. The following 12 combined δ functions can be convolved with a circle function to represent the light field distribution (U) of 12-point light sources in the $x'-y'$ plane,

$$U(x',y') = \left\{\sum_{n=0}^{5}\delta\left[x'-a\cos\left(\frac{n\pi}{3}-\frac{\alpha}{2}\right),y'-a\sin\left(\frac{n\pi}{3}-\frac{\alpha}{2}\right)\right]e^{i\pi} + \sum_{n=0}^{5}\delta\left[x'-a\cos\left(\frac{n\pi}{3}+\frac{\alpha}{2}\right),y'-a\sin\left(\frac{n\pi}{3}+\frac{\alpha}{2}\right)\right]\right\} \otimes \mathrm{circ}\left(\frac{\sqrt{x'^2+y'^2}}{w}\right), \tag{3}$$

where $\alpha = \arctan(\frac{\sqrt{3}}{9})$, $\otimes$ is a symbol of convolution, circ is a circle function, and w stands for the radius of each source hole. After passing the Fourier transform lens, the field distribution (ψ) generated in the focal $x-y$ plane behind the lens is as follows:

$$\psi(x,y) = \left[\sum_{n=0}^{5} e^{\frac{-2i\pi a\cos\left(\frac{n\pi}{3}-\frac{\alpha}{2}\right)x}{\lambda f}} e^{\frac{-2i\pi a\sin\left(\frac{n\pi}{3}-\frac{\alpha}{2}\right)y}{\lambda f}} - \sum_{n=0}^{5} e^{\frac{-2i\pi a\cos\left(\frac{n\pi}{3}+\frac{\alpha}{2}\right)x}{\lambda f}} e^{\frac{-2i\pi a\sin\left(\frac{n\pi}{3}+\frac{\alpha}{2}\right)y}{\lambda f}}\right] \times \left[\frac{\lambda f w J_1\left(2\pi w\sqrt{x^2+y^2}/\lambda f\right)}{\sqrt{x^2+y^2}}\right], \tag{4}$$

where J_1 is the first-order Bessel function, λ is the wavelength of light, and f is the focal length of the Fourier transform lens. The optical field of the observation plane can be represented by the Fraunhofer (Fresnel) diffraction integral when the light transmission distance satisfies $\Delta z > \frac{w^2}{2\lambda}$ ($\Delta z < \frac{w^2}{2\lambda}$).

3. Experimental Results

The periodic moiré wave field is selected as the test field, and its self-healing after the obstacle is shown in Fig. 3 (Figs. 4 and 5). The sizes of the wave field and the obstacle are 3.93 mm × 3.93 mm and 0.78 mm × 0.78 mm, respectively. The CCD camera is positioned at f_0 in the rear focal plane of lens L4 while the obstacle is placed between L4 and f_0 and moves along the z axis. When the obstacle is positioned 25 mm in front of the focal plane (f_0), the center of the wave fields is blocked and there is a dark region, which is similar in size to the obstacle, and its edge is distorted due to diffraction, as shown in Fig. 3(a). When the obstacle is placed 55 mm in front of the focal plane (f_0), the original wave-field structure can be reconstructed in the center of the dark area while the distortion range of the edge of the dark area is expanded, slightly distorting the original structure, as shown in Fig. 3(b). When the obstacle is farther away from the focal plane (f_0), such as 90 and 130 mm, the moiré structure of the blocked area is repaired, and the range of peripheral distortions continues to expand but the degree is reduced, as shown in Figs. 3(c) and 3(d), respectively. Figure 3(d) shows that the self-healing of the light field is complete, where the distance required to repair the information and energy loss caused by the obstacle of this size is reached. The above experimental results confirm that as a large-period two-dimensional light field with a complex structure, the moiré lattice light field has good nondiffraction and self-healing properties.

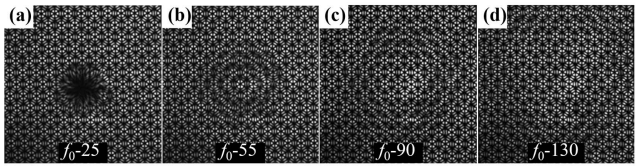

Fig. 3. Self-healing of the wave fields with diameters of obstacle of (a) 25 mm, (b) 55 mm, (c) 90 mm, and (d) 130 mm in front of f_0.

A circular defect with $R = 50$ μm is introduced in the center of the phase diagram loaded in the SLM. The simulated and experimental results of the generated light field at f_0 are shown in Fig. 4(a1); they possess a circular defect corresponding to the phase diagram. Figures 4(a2)–4(a4) show the experiment results of the self-healing transmitting over different distances. With the increase in transmission distance, the six damaged bright spots in the middle of the honeycomb structure first extend inward and are then repaired completely. Self-healing can be achieved by transferring only 25 mm because the defect is small. Comparing the experimental results shown in Figs. 4(a1)–4(a4), it was found that the experimental results were highly consistent with the simulated results. The wave-field patterns for $R =$ 125 μm are shown in Figs. 4(b1)–4(b4). First, the wave field at the edge of defect extends toward the center, forming a "trestle bridge" at the defect region, as shown in Fig. 4(b2). Then the wave field around the defect is darkened and distorted while the original moiré structure (six bright spots) is repaired in the center of the defect [Fig. 4(b3)]. Finally, the area around the defect is repaired, and self-healing is almost completed at 60 mm after f_0, as shown in Fig. 4(b4). The simulated and experimental results show that "the larger the defect size, the longer the transmission distance required to complete the repair[14]."

To verify the universality of self-healing process, the shape and position of the defect were changed, and the experiment was repeated to observe the self-healing process. The triangular defect was formed by removing the unit structure at the center of the moiré lattice field and its left adjacent and upper left positions, as depicted in Figs. 4(c1)–4(c4). The self-healing process is the same as that with circular defects. As the defect area expanded, the minimum self-healing distance increases to about 70 mm. When the defect with radius of $R = 100$ μm deviates

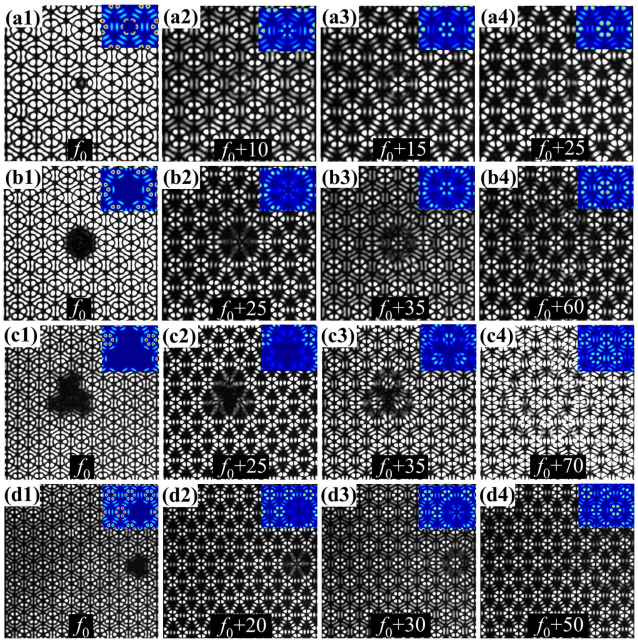

Fig. 4. Self-healing of the wave fields with small defects. (a1) Wave field with defects at R = 50 μm; (a2)–(a4) wave-field experimental results at 10, 15, and 25 mm behind the focal plane; (b1) wave field with defects at R = 125 μm; (b2)–(b4) wave-field experimental results at 25, 35, and 60 mm behind the focal plane; (c1) wave-field experimental diagram of a triangular defect; (c2)–(c4) wave-field experimental diagram at 25, 35, and 70 mm behind f_0; (d1) wave field with defect position far from the center; (d2)–(d4) wave-field experimental results at 20, 30, and 50 mm behind the focal plane. Insets (the blue diagrams in the upper right corner) are the simulated wave-field intensities.

from the center of the wave field, the self-healing process is still from the inside out, independent of the defect location [Figs. 3(d1)–3(d4)]. It shows that the energy and phase information carried in the central region of moiré structures has a stronger anti-interference ability.

Moiré lattice fields generated by the holographic method maintain nondiffraction characteristics well in the range of $(f_0 - 6, f_0 + 15)$ cm[27]. Therefore, the wave field in the nondiffracting region that locates in front of f_0 needs to be investigated. A defect with $R = 125$ μm is set in the center of the moiré wave field. The simulation and experimental results of self-healing of wave fields at different positions before f_0 are shown in Figs. 5(a1)–5(a4) and 5(b1)–5(b4), respectively. The "trestle" structure extends inwards from the defect area at 25 mm in front of f_0. At the end of the trestle, six bright spots are reconstructed at 35 mm in front of f_0. The original moiré structures reappear in the area around the defect at 60 mm in front of f_0. The minimum self-healing distance in the back of f_0 is 60 mm. The self-healing of the wave field at $(f_0 - 60)$ mm is not perfect because of the proximity of the nondiffraction edge. Comparing the above results with Figs. 4(b1)–4(b4), it is easy to see that the self-healing results of moiré lattice fields at equal distances in front of and behind f_0 are similar, indicating that the self-healing process is symmetric about f_0.

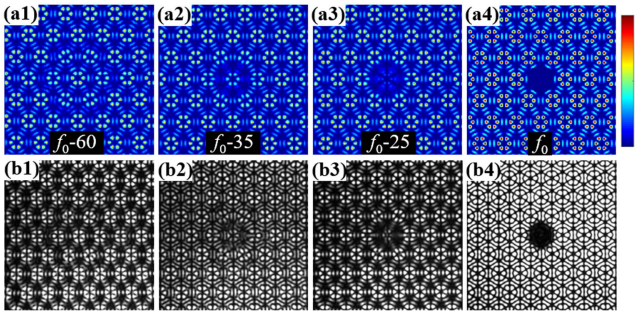

Fig. 5. Intensities of the wave field in front of f_0. (a1)–(a3) Simulated self-healing results at 60, 35, and 25 mm in front of f_0; (a4) wave field with a defect at f_0; (b1)–(b4) experimental results at the corresponding positions.

The transmission distance that just completes the self-healing is called the minimum self-healing distance. To quantify the relationship between self-healing distance and defect size, we introduce the similarity degree[30] as

$$D_p(z) = \frac{\left[\iint I_{\mathrm{wt}}(\rho, z) I_{\mathrm{ob}}(\rho, z) \mathrm{d}^2\rho\right]^2}{\iint I_{\mathrm{wt}}(\rho,z)^2 \mathrm{d}^2\rho \iint I_{\mathrm{ob}}(\rho,z)^2 \mathrm{d}^2\rho}, \tag{5}$$

where ρ is an arbitrary point in the moiré wave field; I_{wt} and I_{ob} stand for the beam intensities without and with obstacles, respectively; and the angular brackets denote ensemble averaging. $D_p = 1$ denotes that the intensity distribution of the field with defects at this position is identical to that without defects. The simulations of the self-healing processes of various moiré lattice wave fields (periodic or aperiodic, honeycomb or square) with defects are shown in Fig. 6, where the 200 mm position is the second focal plane of the 4f system. Clearly, the self-healing process is symmetrical about f_0 and requires a longer distance to complete the repair corresponding to the larger defect. In addition, the value of D_p for different moiré lattice wave fields is close when they possess the same defect, indicating the self-healing process is similar.

Figure 7 shows the experimental measured "$Z_{\min} - R$", which is linearly related to the defect radius. It can be considered that

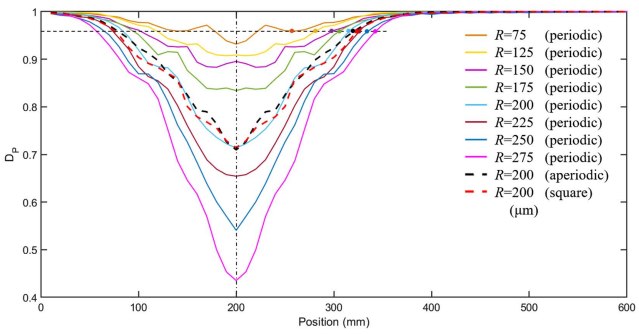

Fig. 6. Simulation of the self-healing process. The solid line describes the self-healing of two periodic moiré lattice wave fields (honeycomb). The black dotted and red dotted lines indicate the self-healing of periodic square moiré lattice wave fields and aperiodic moiré lattice wave fields, respectively.

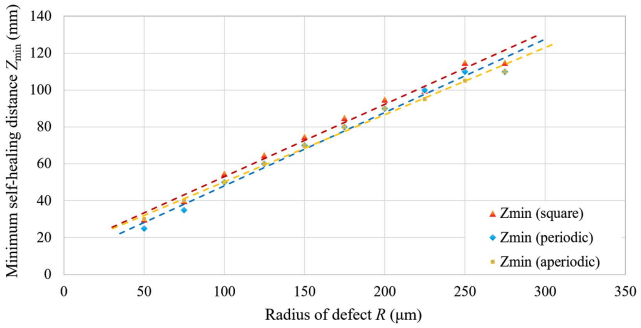

Fig. 7. Linear fitting of minimum self-healing distance.

the minimum self-healing distance of moiré wave fields (periodic or aperiodic, honeycomb or square) is proportional to the radius of the defect (obstacle) in the diffraction-free transmission range. However, when the transmission distance approaches or exceeds the nondiffractive range, the repair effect worsens. Also, the minimal self-healing distance is affected slightly by the periodicity and shape of the moiré lattice wave fields.

4. Conclusion

In conclusion, holographic technology is utilized to design moiré lattice wave fields with defects. The moiré lattice wave fields can recover their original structure at a certain distance after being disturbed by obstacles. The self-healing properties of defects with different sizes, positions, and shapes are studied. In nondiffractive transmission, the self-healing process and principles of the moiré lattice wave fields are summarized as follows. (i) The structure at the center of the defect is repaired first, and then the structure at the edge is repaired. (ii) The minimum self-healing distance $Z_{\min}$ is positively correlated with the radius of the defect. (iii) The self-healing process of moiré wave fields is symmetric concerning f_0 (the second focal plane of the 4f system).

Acknowledgement

This work was supported by the National Key Research and Development Program of China (No. 2019YFA0705000), the National Natural Science Foundation of China (NSFC) (Nos. 12104272, 12192254, 91750201, and 11974218), the Innovation Group of Jinan (No. 2018GXRC010), and the Local Science and Technology Development Project of the Central Government (No. YDZX20203700001766).

References

1. A. Aiello, G. S. Agarwal, M. Paúr, B. Stoklasa, Z. Hradil, J. Řeháček, P. de la Hoz, G. Leuchs, and L. L. Sánchez-Soto, "Unraveling beam self-healing," Opt. Express **25**, 19147 (2017).
2. Z. Bouchal, J. Wagner, and M. Chlup, "Self-reconstruction of a distorted nondiffracting beam," Opt. Commun. **151**, 207 (1998).
3. V. Garcés-Chávez, D. McGloin, M. Summers, A. Fernandez-Nieves, G. C. Spalding, G. Cristobal, and K. Dholakia, "The reconstruction of optical angular momentum after distortion in amplitude, phase and polarization," J. Opt. A **6**, S235 (2004).
4. M. Vasnetsov, I. Marienko, and M. Soskin, "Self-reconstruction of an optical vortex," J. Exp. Theor. Phys. Lett. **71**, 130 (2000).
5. R. MacDonald, S. Boothroyd, T. Okamoto, J. Chrostowski, and B. Syrett, "Interboard optical data distribution by Bessel beam shadowing," Opt. Commun. **122**, 169 (1996).
6. J. Durnin, J. Miceli, Jr., and J. H. Eberly, "Diffraction-free beams," Phys. Rev. Lett. **58**, 1499 (1987).
7. J. Durnin, "Exact solutions for nondiffracting beams. I. The scalar theory," J. Opt. Soc. Am. A **4**, 651 (1987).
8. D. McGloin and K. Dholakia, "Bessel beams: diffraction in a new light," Contemp. Phys. **46**, 15 (2005).
9. M. Anguiano-Morales, M. M. Mendez-Otero, M. D. Iturbe-Castillo, and S. Chávez-Cerda, "Conical dynamics of Bessel beams," Opt. Eng. **46**, 078001 (2007).
10. P. Vaity and R. Singh, "Self-healing property of optical ring lattice," Opt. Lett. **36**, 2994 (2011).
11. R. Cao, Y. Hua, C. Min, S. Zhu, and X. C. Yuan, "Self-healing optical pillar array," Opt. Lett. **37**, 3540 (2012).
12. V. Dev and V. Pal, "Divergence and self-healing of a discrete vortex formed by phase-locked lasers," J. Opt. Soc. Am. B **38**, 3683 (2021).
13. P. Zhang, Y. Hu, T. Li, D. Cannan, X. Yin, R. Morandotti, Z. Chen, and X. Zhang, "Nonparaxial Mathieu and Weber accelerating beams," Phys. Rev. Lett. **109**, 193901 (2012).
14. X. Chu, G. Zhou, and R. Chen, "Analytical study of the self-healing property of Airy beams," Phys. Rev. A **85**, 013815 (2012).
15. L. Zhang, F. Ye, M. Cao, D. Wei, P. Zhang, H. Gao, and F. Li, "Investigating the self-healing property of an optical Airy beam," Opt. Lett. **40**, 5066 (2015).
16. B. Y. Wei, P. Chen, S. J. Ge, W. Duan, W. Hu, and Y.-Q. Lu, "Generation of self-healing and transverse accelerating optical vortices," Appl. Phys. Lett. **109**, 121105 (2016).
17. S. Chávez-Cerda, J. Gutiérrez-Vega, and G. New, "Elliptic vortices of electromagnetic wave fields," Opt. Lett. **26**, 1803 (2001).
18. M. A. Bandres, J. C. Gutiérrez-Vega, and S. Chávez-Cerda, "Parabolic nondiffracting optical wave fields," Opt. Lett. **29**, 44 (2004).
19. M. Anguiano-Morales, A. Martínez, M. D. Iturbe-Castillo, S. Chávez-Cerda, and N. Alcalá-Ochoa, "Self-healing property of a caustic optical beam," Appl. Opt. **46**, 8284 (2007).
20. Y. Gao, Z. Wen, L. Zheng, and L. Zhao, "Complex periodic non-diffracting beams generated by superposition of two identical periodic wave fields," Opt. Commun. **389**, 123 (2017).
21. M. Kumar and J. Joseph, "Embedding a nondiffracting defect site in helical lattice wave-field by optical phase engineering," Appl. Opt. **52**, 5653 (2013).
22. S. K. Pal and P. Senthilkumaran, "Lattice of C points at intensity nulls," Opt. Lett. **43**, 1259 (2018).
23. C. Huang, F. Ye, X. Chen, Y. V. Kartashov, V. V. Konotop, and L. Torner, "Localization-delocalization wavepacket transition in Pythagorean aperiodic potentials," Sci. Rep. **6**, 32546 (2016).
24. P. Wang, Y. Zheng, X. Chen, C. Huang, Y. V. Kartashov, L. Torner, V. V. Konotop, and F. Ye, "Localization and delocalization of light in photonic moiré lattices," Nature **577**, 42 (2020).
25. Q. Fu, P. Wang, C. Huang, Y. V. Kartashov, L. Torner, V. V. Konotop, and F. Ye, "Optical soliton formation controlled by angle twisting in photonic moiré lattices," Nat. Photon. **14**, 663 (2020).
26. J. W. Fleischer, M. Segev, N. K. Efremidis, and D. N. Christodoulides, "Observation of two-dimensional discrete solitons in optically induced nonlinear photonic lattices," Nature **422**, 147 (2003).
27. C. Shang, C. Lu, S. Tang, Y. Gao, and Z. Wen, "Generation of gradient photonic moiré lattice fields," Opt. Express **29**, 29116 (2021).
28. A. Aiello and G. S. Agarwal, "Wave-optics description of self-healing mechanism in Bessel beams," Opt. Lett. **39**, 6819 (2014).
29. M. Ornigotti and A. Aiello, "Radially and azimuthally polarized nonparaxial Bessel beams made simple," Opt. Express **21**, 15530 (2013).
30. Z. Xu, X. Liu, Y. Chen, F. Wang, L. Liu, Y. E. Monfared, S. A. Ponomarenko, Y. Cai, and C. Liang, "Self-healing properties of Hermite-Gaussian correlated Schell-model beams," Opt. Express **28**, 2828 (2020).